ORIGINAL ARTICLE

Unraveling the complexities of a highly heterogeneous aquifer under convergent radial flow conditions

Guglielmo Federico Antonio Brunetti[1] · Mario Maiolo[1] · Carmine Fallico[2] · Gerardo Severino[3]

Abstract

Untangling flow and mass transport in aquifers is essential for effective water management and protection. However, understanding the mechanisms underlying such phenomena is challenging, particularly in highly heterogeneous natural aquifers. Past research has been limited by the lack of dense data series and experimental models that provide precise knowledge of such aquifer characteristics. To bridge this gap and advance our current understanding, we present the findings of a pioneering experimental investigation that characterizes a unique, strongly heterogeneous, laboratory-constructed phreatic aquifer at an intermediate scale under radial flow conditions. This strong heterogeneity was achieved by randomly distributing 2527 cells across 7 layers, each filled with one of 12 different soil mixtures, with their textural characteristics, porosity, and saturated hydraulic conductivity measured in the laboratory. We placed 37 fully penetrating piezometers radially at varying distances from the central pumping well, allowing for an extensive pumping test campaign to obtain saturated hydraulic conductivity values for each piezometer location and scaling laws along eight directions. Results reveal that the aquifer's strong heterogeneity led to significant vertical and directional anisotropy in saturated hydraulic conductivity. Furthermore, we experimentally demonstrated for the first time that the porous medium tends toward homogeneity when transitioning from the scale of heterogeneity to the scale of investigation. These novel findings, obtained on a uniquely highly heterogeneous aquifer, contribute to the field and provide valuable insights for researchers studying flow and mass transport phenomena. The comprehensive dataset obtained will serve as a foundation for future research and as a tool to validate findings from previous studies on strongly heterogeneous aquifers.

1 Introduction

Understanding and predicting water flow and mass transport in groundwater is crucial for managing and protecting water resources essential for human life. This knowledge enables actions such as remediation of polluted sites, significantly impacting environmental, social, and economic sustainability.

✉ Guglielmo Federico Antonio Brunetti
guglielmo.brunetti@unical.it

1 Department of Environmental Engineering, University of Calabria, Rende, Italy

2 Department of Civil Engineering, University of Calabria, Rende, Italy

3 Department of Agricultural Sciences, University of Naples-Federico II, Naples, Italy

Traditionally, water flow in porous media is described using classic flow equations, assuming constant aquifer parameters within the investigated domain [1]. However, natural aquifers often exhibit spatial heterogeneity in their hydrogeological properties [2], affecting water flow and mass transport in various ways and at different scales, thereby hindering our understanding of the mechanisms underlying these phenomena. Such properties may differ from point to point in the investigated site, causing the intrinsic structure of the entire porous medium to be variable. As a result, spatially variable hydraulic parameters, such as hydraulic conductivity, can often be treated as Random Space Functions (RSFs), with flow equations modeled as stochastic [3–7]. Hereafter in the text, the term 'hydraulic conductivity' will always refer to saturated conditions. A statistical approach, justified by the uncertainty characterizing these parameters, allows for the description of the spatial structure of these RSFs

using Probability Density Functions (PDFs) of known values at a limited number of points. The more numerous the aquifer locations with known hydraulic parameters, the more reliable the water flow description provided by the equations. However, aquifer characterization often involves considering the average values of characteristic parameters determined through direct field measurements or laboratory samples, which can generally only be carried out at a limited number of locations. This circumstance introduces random errors [8], causing uncertainty in the study of flow and transport phenomena [9, 10].

The complexity in describing such phenomena is further compounded by the fact that heterogeneity often renders the medium anisotropic, meaning the vector variation of the physical properties of the investigated domain [11]. This is an aspect that requires careful verification, as there are cases of aquifers that are homogeneous and anisotropic or even heterogeneous and isotropic.

In any case, heterogeneity and anisotropy, which strongly influence water flow within a porous aquifer, depend on the particular scale to which they refer [12]. For scales larger than that at which the porous medium is heterogeneous, the same porous medium can often be considered homogeneous, isotropic, or anisotropic [13]. At smaller scales, traditionally defined as laboratory scales with the characteristic dimensions of soil samples (between a few centimeters up to 40-50 cm), heterogeneity manifests its influence mainly through geometry, size, and orientation of grains and pores, as well as other factors such as various chemical-physical processes between fluid and solid matrix (dissolution, precipitation) and mechanical processes like compaction [14–16]. Microstratification, foliation, cracks, and plant roots are also possible sources of heterogeneity at this scale. At larger scales, such as the field scale, heterogeneity's influence is mainly induced by the presence of layers with different permeability, stratification, tortuosity, and the interconnection and continuity of flow paths and canaliculi [6, 17–24].

Among the many relevant aspects in studying heterogeneity, understanding hydraulic conductivity behavior under different flow conditions is of great importance [25–28]. In particular, the study of radial flow generated through pumping wells is of significant interest in hydrogeology [22, 29, 30], as under these conditions, remediation actions and field measurements of hydraulic parameters are generally performed. To address the significant impact of natural aquifers' heterogeneity over this flow condition, a common approach is to identify and define a homogeneous (fictitious) aquifer with proper upscaled hydraulic conductivity representative of the heterogeneous formation [25, 31–34]. In this context, the non-uniform conditions generated in the region surrounding the well [6, 35], and the flow mechanisms in the near and far-field, do not allow one to consider the estimated effective conductivity, which is only definable under conditions of mean uniform head gradient [36], as a medium property. Thus, the concepts of equivalent conductivity, concerning the spatial averages of flows [37, 38], and apparent conductivity, concerning the mean flux and mean head gradient, were introduced [6, 39–41].

The aims of this study consist of experimentally investigating the influence that strong heterogeneity, with which a phreatic aquifer was built in the laboratory, exerts on the main parameters, such as hydraulic conductivity, which govern the water flow inside the saturated porous medium. The study also aims to verify whether this strong heterogeneity made the porous medium anisotropic, referring the results obtained to the particular scale of investigation, i.e., the intermediate (meso)-scale. At this scale, which acts as a link between the laboratory and the field scales [42, 43], the influence of heterogeneity occurs with both the modalities typical of the other two extreme scales, making it easier to interpret, albeit with undeniable uncertainty, how particular (i.e. local) phenomena often influence water flow and mass transport at larger (macro) scales [44–46]. For this reason, knowing the structure of the porous medium at the mesoscale, i.e., textural characteristics, porosity, and hydraulic conductivity, is of fundamental importance in characterizing the transition between the other two extreme scales. Furthermore, it is essential to note that many practical water management actions and the occurrence of contaminated aquifer volumes typically fall within the intermediate scale range. In this study, we define the laboratory scale as that characterized by the dimensions of permeameters or flow columns commonly used in laboratories (from about 0.1 m to about 0.6 m), while the field scale is characteristic of external spaces, with distances greater than 5 m - 10 m. Moreover, we aim to verify whether, at a scale larger than that of heterogeneity, the porous medium under consideration tends towards homogeneity. It is necessary to underline that the present study, due to the fact that it was carried out on an artificially packed strongly heterogeneous formation, is unique [32]. Indeed, some similar pre-existing studies refer only to mildly heterogeneous porous media created in a laboratory [47]. It is evident that the theoretical results deriving from the experimentation on a device reproducing a highly heterogeneous aquifer, such as the one considered in the present study, can be extended to highly heterogeneous natural formations, with significant benefits for the entire scientific community.

In the following section, we will describe the various construction phases of the aquifer under consideration. Subsequently, we will present the methodologies used to determine total and effective porosity, horizontal and vertical hydraulic conductivity, anisotropy, and scaling laws of K in various directions. Afterward, we will report the results obtained during the experimental investigation, along with an in-depth discussion. Finally, we will present

the conclusions, summarizing the results and key aspects of the study.

2 Materials

The experimental apparatus, designed to contain the highly heterogeneous aquifer under investigation, was constructed at the "Grandi Modelli Idraulici" Laboratory of the University of Calabria. The system consists of a 2 m × 2 m × 1 m metal box, with its walls suitably reinforced using stiffening elements. A 5 cm-thick perimeter chamber was formed along the entire inner border of the box by attaching a metal mesh to appropriate metal supports and overlaying a layer of geotextile. This design allows for the containment of the porous medium that composes the aquifer, while simultaneously enabling water to flow freely outward into the chamber (Fig. 1).

Experimental tests were carried out using this system configuration, allowing for verification of compliance with boundary conditions and monitoring of the predetermined hydraulic head's constancy.

To ensure the precise fixation of the latter, the perimeter chamber was connected to two small, height-adjustable PVC tanks located on opposite walls of the experimental apparatus, each containing a rectangular weir. Additionally, 37 fully-penetrating piezometers, each with a radius of 0.014 m, were installed within the box following a radial pattern centered around the central pumping well. To achieve maximum accuracy in replicating this layout, a tracing operation was performed on the metal box's bottom. Each 0.5 m high piezometer was preliminarily screened through the entire 0.3 m thickness of the saturated layer and covered with a geotextile material to allow water flow while preventing solid particle intrusion. Figure 2 presents the planimetric scheme of the experimental apparatus, including the arrangement of the central well and various piezometers,
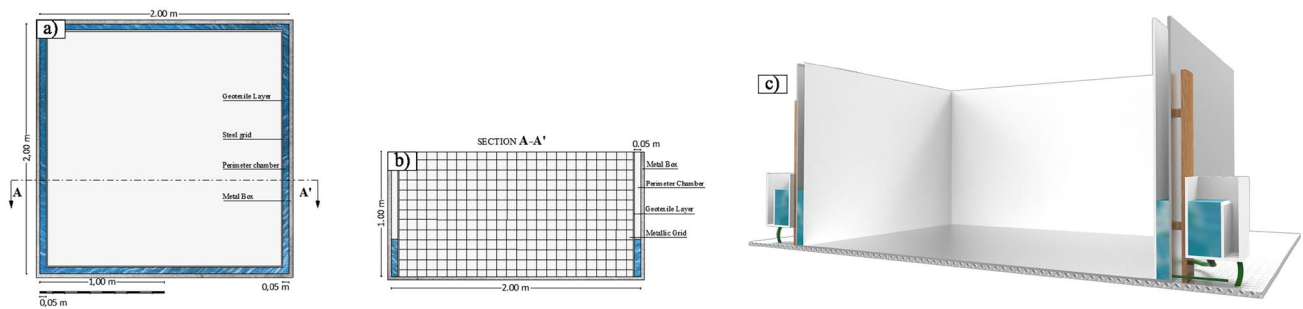

Fig. 1 a Experimental device plan view. **b** Cross-sectional representation of the device. **c** 3D visualization of the experimental setup, highlighting the perimeter chamber and its connection to two height-adjustable PVC tanks
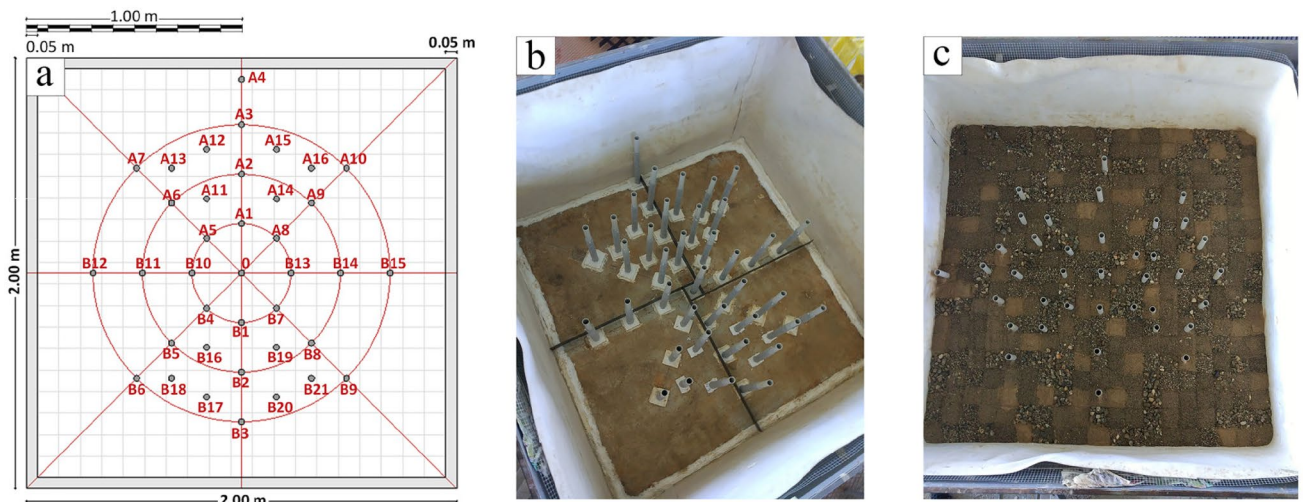

Fig. 2 a Planimetric diagram of the box displaying the arrangement of the central well and the various piezometers. **b** Photograph of the bottom of the box, featuring the central well and installed piezometers. **c** Photo of the upper surface of the completed aquifer (7th layer)

as well as a photograph of the installed piezometers. A detailed planimetric layout of the device is also provided in the accompanying Supplementary Material (Fig. SM1).

The medium was artificially packed in the device in order to reproduce a statistical distribution of $Y \equiv \ln K$ of variance of Y, i.e. , $\sigma_Y^2 = 3.79$, a value typical of the so called *strongly heterogeneous media* [32].

A configuration consisting of seven porous layers, each with a thickness of 0.05 meters and comprising 361 cells (arranged in a 19 x 19 matrix), with each cell measuring $0.1\,\text{m} \times 0.1\,\text{m} \times 0.05\,\text{m}$, was constructed. Consequently, the aquifer is composed of a total of 2527 cells, with each cell being filled with one of twelve different soil mixtures. The arrangement of these materials was generated according to a uniform random distribution, which resulted in a lack of correlation among the cells. Thus, the autocorrelation function $\rho(x)$ exhibits a pattern characteristic of what are termed 'structureless formations' [10]. To better clarify this aspect, we examine the relative distance x between any two points within the aquifer, alongside the integral scale L, which denotes either the horizontal (I) or the vertical (I_v) integral scale. In the described aquifer, the integral scales correspond to the dimensions of the cells (namely, I is about 10 cm and I_v is about 5 cm) [32]. When $x > L$, the autocorrelation function $\rho(x)$ equals 0, and the values of K at these points will differ significantly. Conversely, any two points within the aquifer will exhibit identical K values when $x < L$, and the autocorrelation function $\rho(x)$ becomes 1.

The NumPy library (Python programming language) was used to assign to each layer a, randomly selected, conductivity-value by means of the following commands:

```
import random

import numpy as np

x = str(np.random.randint(1, 13, size=(19, 19)))
```

The figures SM2 and SM3 in the supplementary materials respectively show the exact arrangement of each material cell in the 7 layers and a histogram of the hydraulic conductivity values relative to the generated uniform distribution.

The following Fig. 3 illustrates the cross-sectional view of the experimental device built in the laboratory, as well as the overlapping layers that form the aquifer.

Each soil type (TI, TII, TIII, TIV, TV, TVI, TVII, TVIII, TIX, TX, TXI, TXII) composing the aquifer corresponds to a unique mixture created by combining various quantities of silt, sand, fine gravel, and coarse gravel. These porous material mixtures were subject to comprehensive grain size analysis, which defined the granulometric curve for each soil type. Additionally, the effective grain diameters d_{10} and d_{60} (particle size for which 10% and 60% of the examined sample are finer than), the uniformity coefficient of grains ($U = d_{60}/d_{10}$), total porosity and effective porosity were also determined. The hydraulic conductivity of all 12 soil types was assessed in the laboratory.

To effectively and conveniently arrange each porous material cell within the device without leaving any gaps or causing other disturbances, we designed two elements. A "cruciform" metal element temporarily divided the laying area of each stratum into four sections, while a $1.0 \times 0.9 \times 0.05$ m metal grid (with a surface area equal to one quarter of the entire caisson's surface) featured mesh dimensions precisely matching those of a porous cell (Fig. 4, first image). The grid was initially positioned in one of the quarters (Fig. 4, second image) and subsequently removed upon the completion of cells placement. It was then relocated nearby and the filling process was repeated until an entire layer was formed (Fig. 4, third image). After completing the layer, the cruciform element was also removed. To promote compaction and eliminate any potential gaps between adjacent inclusions or air bubbles, multiple wetting cycles were applied. This procedure was repeated seven times to construct the entire aquifer (Fig. 4, fourth image). It is essential to note that the placement
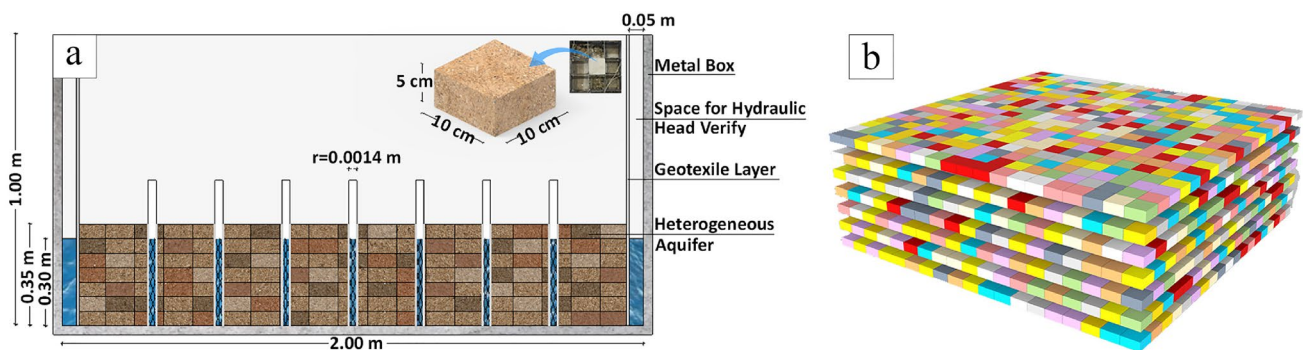

Fig. 3 **a** Cross-sectional view of the experimental device constructed in the laboratory, with a single cell highlighted. **b** Random distribution of the soil types that make up the aquifer and overlapping layers

Fig. 4 Illustration (from left to right) depicting the sequence that forms the layers of cells constituting the geological formation. Reproduced with permission from Brunetti et al. [32], (adapted from Figure 2 of the original article)

of inclusions occurred with the piezometers already installed (Fig. 4, first image), ensuring that there were no disturbances due to the application of piezometers.

Figure 5 presents the final configuration of the experimental setup, which includes the aquifer [32]. To ensure a consistent water level in the perimeter chamber during pumping (*a*, Fig. 5), a marginally elevated flow rate was introduced from the bottom of the container (*b*, Fig. 5). Overflow prevention was achieved by hydraulically connecting the chamber to a pair of tanks (*c*, Fig. 5) with their water levels set at 30 cm and stabilized by an internal weir. Pressure transducers situated at the base of each well facilitated the gathering of precise hydraulic head data.

3 Methods

3.1 Measurements of porosity on soil samples

Total porosity measurements were carried out on samples of porous media mixtures corresponding to each of the 12 soil types that make up the aquifer. These measurements were obtained using the following relationship [48, 49]:

$$n = 1 - \frac{\rho_{\text{bulk}}}{\rho_{\text{grain}}} \tag{1}$$

where ρ_{bulk} represents the bulk mass density [ML^{-3}] and ρ_{grain} denotes the particle mass density [ML^{-3}].
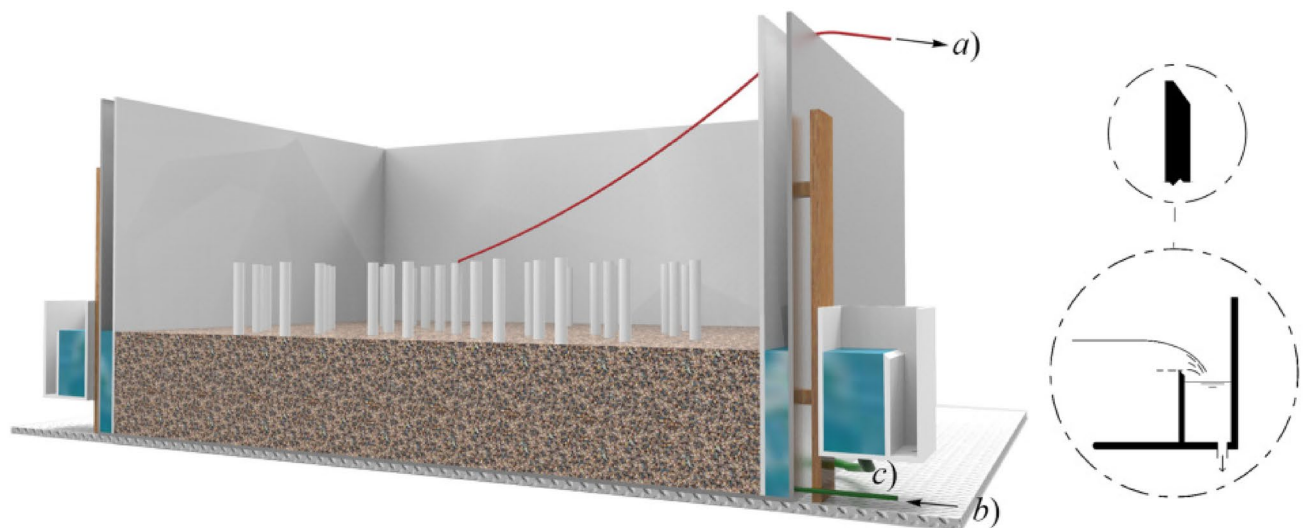

Fig. 5 A three-dimensional perspective of the experimental setup is provided, along with the apparatus implemented to establish the specified head boundary condition surrounding the aquifer. Reproduced with permission from Brunetti et al. [32], (adapted from Figure 5 of the original article)

The effective porosity (the difference between saturated water content and residual water content) was determined using the following relationship, as described by Staub et al. [50]:

$$n_e = n - \frac{V_w}{V} \tag{2}$$

where V is the total volume $[L^3]$ and V_w represents the volume of water that cannot be drained by gravity $[L^3]$, under equilibrium conditions at 33 kPa of suction, as reported by Ahuja et al. [51].

3.2 Measurements of hydraulic conductivity on soil samples

During the device's construction phase, specific samples were prepared in the laboratory for each of the 12 types of porous media constituting the aquifer. Hydraulic conductivity (K) measurements were carried out on these samples using flux cells as constant head permeameters. Each soil sample was cylindrical in shape, matching the internal dimensions of the flux cells used for K measurements, with a diameter of 0.064 m and a height of 0.30 m.

The measuring device comprises a cell in which the soil sample, pre-saturated with water, is placed. The cylindrical wall of the cell is made of plexiglas, while the lower and upper bases consist of two porous membranes positioned on circular meshes that serve as support and facilitate water flow. The cell's lower surface is connected by a Tygon tube to a Mariotte bottle for fixing the hydraulic head, while another Tygon tube enables water to exit from the upper surface, ensuring the release of air trapped within the soil sample.

Hydraulic conductivity were measured considering hydraulic heads ranging from 0.05 to 1 m, as suggested by Klute et al. [52]. For each of the 12 soil types, the K measurement was repeated three times, with the average value considered as the representative one. The K values obtained through the above-described method on soil samples are representative of the vertical hydraulic conductivity, in accordance with the direction of water flow within the sample [53, 54].

3.3 Measurement of hydraulic conductivity by pumping test

Following the construction of the heterogeneous aquifer, numerous pumping tests were carried out, each involving constant flow rate pumping from the central well. The tests were repeated with 10 different pumping rates (20 L/h, 25 L/h, 30 L/h, 35 L/h, 40 L/h, 47.5 L/h, 50 L/h, 55 L/h, 60 L/h, 70 L/h). For each test, the hydraulic conductivity (K) values

in the piezometers (refer to Fig. 2) were determined using Neuman's method [55]. In some cases, when the detected head values were challenging to interpret using Neuman's method, Jacob's method [56] was utilized instead, ensuring a more accurate analysis. Additionally, compliance with the assumptions imposed by the particular method adopted for analyzing hydraulic head variations over time, under unsteady state flow conditions, was verified for each test. The boundary conditions for these methods primarily involve assuming the aquifer to have infinite lateral extension, isotropic or anisotropic with uniform thickness, hydraulic conductivity oriented parallel to the coordinated axes, fully penetrating well, and constant rate pumping. To treat the aquifer as having unlimited extension, the hydraulic head values must remain undisturbed near the metallic box's edge during pumping. This necessitated performing tests with very low flow rates, enabling experimental verification of head invariance in the piezometers farthest from the central pumping well and, consequently, closer to the aquifer's limit. In any case, as the aquifer is unconfined, the very low pumping rates allowed for the vertical component of velocity to be neglected in the points closest to the central well, and, consequently, for the hydraulic conductivity to be considered oriented horizontally.

During the tests, the radii of influence (R) were directly measured for the specified flow rates. To determine these R values, we considered the farthest point on the boundary of the depression cone that formed during pumping, which schematically represents the aquifer's free surface within the axial section of the cone. This portion of the connecting line with the undisturbed level of the aquifer can be identified by the last two piezometers where a change in head was detected. This last part of the depression cone can be approximated as nearly straight, even for very small flow rates. For a time (t) close to steady-state conditions, the non-zero head values in the two aforementioned piezometers are known, and the straight line representing the last part of the depression cone remains well-defined. This line can be drawn, and its intersection with the horizontal line representing the undisturbed level of the aquifer can be identified. The intersection point is located between the first piezometer, starting from the axis of the pumping well, where no change in hydraulic head was detected, and the one immediately preceding it, where a change in head was still detected. This point indicates the distance from the well axis beyond which pumping has no effect and was assumed to be equal to the radius of influence (R).

It is important to note that the data analysis methods consider a homogeneous aquifer in their assumptions and boundary conditions. Given the high heterogeneity of the aquifer in question, it must be understood that the K values determined by pumping tests should be regarded as representative of the effective hydraulic conductivity [34, 57, 58].

As already clarified, to determine the K values, Neuman's [55] interpretative method was employed, given that the considered aquifer is unconfined. In some cases, Jacob's [56, 59] method was also used. Neuman's method [55] is a curve matching method, defined by the following equation:

$$s(r,t) = \frac{Q}{4\pi T} \int_0^\infty 4y J_0\left(y\beta^{1/2}\right) \left[u_0(y) + \sum_{n=1}^\infty u_n(y)\right] dy \quad (3)$$

where s represents the drawdown [L]; J_0 denotes the Bessel function of order zero and of the first kind; B refers to the thickness of the aquifer [L]; r is the well-piezometer distance [L]; $\beta = \frac{r^2}{B^2}\frac{K_v}{K_h}$ [–]; K_h and K_v are the horizontal and vertical hydraulic conductivity, respectively [LT^{-1}]; $u_0(y)$ and $u_n(y)$ are functions that depend on the complete or incomplete penetration of the well.

Jacob's method [56] posits that the variation trend of the hydraulic head over time, for high time values $(t/r^2 > 5S/T)$, can be expressed by the following equation:

$$s(r,t) = \frac{Q}{4\pi T} \log 2.25 \frac{Tt}{Sr^2} \quad (4)$$

where s is the drawdown [L]; Q represents the pumping rate [L^3T^{-1}]; T refers to the transmissivity [L^2T^{-1}]; S denotes the storativity [–]; t is the time [T]; r is the well-piezometer distance [L]. For the determination of K using the aforementioned methods, the AQTESOLV Pro software [60] was employed.

3.4 Evaluating aquifer anisotropy

When considering a heterogeneous and anisotropic medium, the general flow equation can be represented as follows:

$$\frac{\partial}{\partial x}\left(K_x \frac{\partial h}{\partial x}\right) + \frac{\partial}{\partial y}\left(K_y \frac{\partial h}{\partial y}\right) + \frac{\partial}{\partial z}\left(K_z \frac{\partial h}{\partial z}\right) = S_s \frac{\partial h}{\partial t} \quad (5)$$

In this equation, x, y, z denote the Cartesian coordinate axes, h represents the hydraulic head [L], S_s signifies specific storage [L^{-1}], and K_x, K_y and K_z are the components of hydraulic conductivity corresponding to the Cartesian axes [LT^{-1}]. Additionally, t denotes time [T] [61]. Assuming a Cartesian reference system with a designated origin, Eq. (5) demonstrates that, in the context of a heterogeneous and anisotropic medium, hydraulic conductivity not only varies by direction but also changes according to the coordinates, meaning it differs from point to point. Similarly, when considering the hydraulic conductivity tensor for a heterogeneous and anisotropic medium, the components of K vary spatially from one point to another.
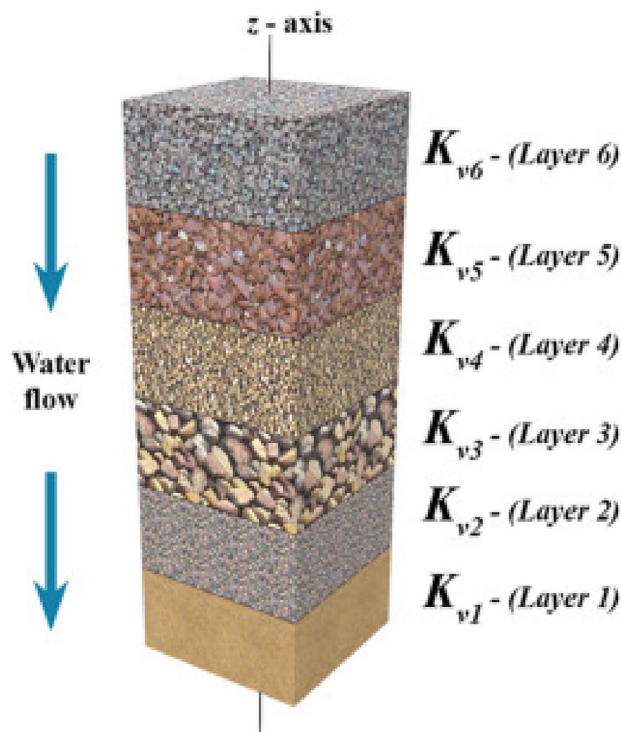

Fig. 6 Diagram illustrating the method for calculating vertical hydraulic conductivity at each well or piezometer location

$$\begin{vmatrix} K_{xx} & K_{xy} & K_{xz} \\ K_{yx} & K_{yy} & K_{yz} \\ K_{zx} & K_{zy} & K_{zz} \end{vmatrix} \quad (6)$$

In general, the heterogeneity of a porous medium does not necessarily imply its anisotropy as well [11]. Thus, for the highly heterogeneous aquifer under investigation, it was crucial to examine the potential anisotropic behavior of the hydraulic conductivity. To accomplish this, the anisotropy ratio (ρ_a), defined by the following relationship, was determined for each considered pumping rate, in correspondence to the central well and each piezometer:

$$\rho_a = \frac{K_v}{K_h} \quad (7)$$

where K_v and K_h represent the vertical and horizontal hydraulic conductivity, respectively.

So, it was necessary to know the vertical hydraulic conductivity corresponding to the central well and each piezometer, having assumed, as described earlier, that the horizontal hydraulic conductivity was equal to the one determined by the pumping tests. To achieve this, similar to the approach used for stratified soils, the vertical hydraulic conductivity value (K_v') was assumed to be the average of the values corresponding to the different layers intersected

or the cells crossed by the piezometer axis along the vertical direction of each well or piezometer (see, Fig. 6).

Consequently, the K'_v values can be obtained using the following relationship:

$$K'_v = \frac{\sum_1^6 K_{v_i}}{6} \tag{8}$$

In this relationship, K_{v_i} represents the vertical hydraulic conductivity of the individual i-th layer [LT^{-1}], measured on the laboratory sample corresponding to the soil type associated with the i-th cell. In the case under investigation, the thickness values of the individual cells along all the verticals of the wells and piezometers are equal to 0.05 m, given that the thickness of the saturated part of the aquifer is 0.30 m. It should be noted that the average value K'_v provided by Eq. (8) is inherently influenced by the direction of water flow. In fact, since this direction is orthogonal to the layer crossed, the average value of the hydraulic conductivity is predominantly affected by the fine-grained layers, i.e. , those with lower hydraulic conductivity. At the end, the values of the anisotropy ratio were determined and meticulously analyzed, resulting in the calculation of the main corresponding statistical parameters.

3.5 Impact of heterogeneity on the scaling behavior of hydraulic conductivity (K)

The heterogeneity of porous media has long been considered the foundation of the scaling behavior of hydraulic conductivity, as confirmed by numerous well-known studies in the literature [21, 42, 62, 63]. Therefore, it is particularly intriguing to verify whether the scaling behavior of K is also present in the highly heterogeneous aquifer considered in this study. For the case at hand, this behavior was investigated, beginning with the central well and following eight directions, ranging from D1 to D8, each separated by an angle of 45°, as depicted in Fig. 7.

Each direction corresponds to an aquifer volume with a horizontal section shaped as a circular sector centered on the pumping well's axis. This sector has a central angle (θ) of 45° and a radius (r) equal to the distance between the axis of the considered piezometer and the central pumping well's axis (see Fig. 8). In the attached supplementary material, the division of the aquifer into sectors is illustrated (Figure SM4). For each of these directions and for each pumping rate, the K values measured at the corresponding piezometers were considered, and the related scaling laws were identified. For this purpose, a power-type law was employed. While the possibility of representing the scaling behavior of a hydraulic parameter using different types of laws cannot be ruled out, the use of a power-type law is often preferred due
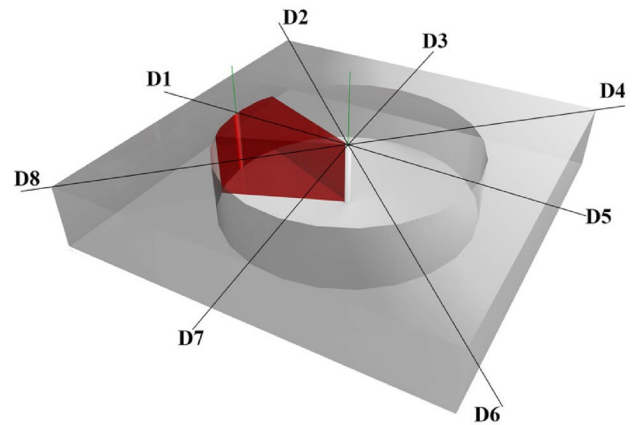

Fig. 7 Aquifer volume associated with one of the eight direction

to its superior representation of experimental data, according to the following expression:

$$P = a \cdot x^b \tag{9}$$

where, P represents the examined parameter (in this case, hydraulic conductivity [LT^{-1}]), x is the scale parameter (distance from the central well [L]), a is a parameter indicative of the structure and heterogeneity of the medium, with dimensions identical to P (in this case, [LT^{-1}]), and b [-] is the so-called "scaling index" (or crowding index) that considers the type of flow within the porous medium and the actual dimensions of the measurement scale [62].

4 Results

The grain size analysis of the soil types that make up the aquifer yielded the corresponding granulometric curves, which are defined by the percentage values of silt, sand, fine gravel, and coarse gravel, as presented in Table 1. This table also displays the effective diameter values d_{10} and d_{60}, as well as the uniformity coefficient ($U = d_{60}/d_{10}$).

Based on Eqs. 1 and 2, the total porosity (n) and effective porosity (n_e) values for the soil types that constitute the aquifer were determined. Additionally, for each of these soil types, samples were prepared and subjected to hydraulic conductivity measurements using flux cells, as previously described. The K_v value for each sample was obtained as the average of three consecutive measurements. Table 2 presents the values of n, n_e, and K_v related to the 12 soil types considered.

The K_v values determined in the laboratory were statistically analyzed, and the main statistical parameters are presented in Table 3 [64].

Table 1 Percentage values of silt, sand, fine gravel, and coarse gravel for each of the 12 soil types comprising the aquifer, along with the corresponding values of the effective diameters d_{10} and d_{60}, and the uniformity coefficient

Soil type	Silt (%)	Sand (%)	Fine gravel (%)	Coarse gravel (%)	d_{10} (mm)	d_{60} (mm)	$U = d_{60}/d_{10}$
T I	–	–	50.00	50.00	2.70	12.50	4.63
T II	–	–	100.00	–	2.80	6.00	2.14
T III	0.25	27.75	–	72.00	0.39	18.50	47.44
T IV	–	46.00	27.00	27.00	0.27	5.05	18.70
T V	–	87.00	13.00	–	0.14	0.80	5.71
T VI	5.80	60.20	17.00	17.00	0.18	1.40	7.78
T VII	5.00	77.00	9.00	9.00	0.20	1.00	5.00
T VIII	0.15	99.85	–	–	0.12	0.72	6.00
T IX	5.70	94.30	–	–	0.14	0.79	5.64
T X	–	44.00	56.00	–	0.41	10.00	24.39
T XI	13.00	87.00	–	–	0.04	0.50	12.50
T XII	38.00	62.00	–	–	0.005	0.37	74.00

Table 2 Total porosity (n), effective porosity (n_e) and hydraulic conductivity (K_v) values for each considered soil type

Soil type	n	n_e	K_v (m/s)
T I	0.50	0.06	3.75e-4
T II	0.62	0.08	3.66e-4
T III	0.29	0.05	6.86e-5
T IV	0.33	0.06	3.44e-3
T V	0.45	0.06	7.49e-5
T VI	0.39	0.05	8.61e-5
T VII	0.45	0.06	1.32e-5
T VIII	0.45	0.07	6.32e-5
T IX	0.47	0.06	2.09e-5
T X	0.39	0.06	2.41e-4
T XI	0.52	0.07	8.56e-6
T XII	0.67	0.07	2.66e-6

Table 4 Piezometers belonging to each sector represented by the eight considered directions

Directions	Piezometers
D1	O, A1, A2, A3, A15, A12
D2	O, A8, A9, A10, A14, A16
D3	O, B13, B14, B15
D4	O, B7, B8, B9, B19, B21
D5	O, B1, B2, B3, B17, B20
D6	O, B4, B5, B6, B16, B18
D7	O, B10, B11, B12
D8	O, A5, A6, A11, A13

Table 3 Main statistical parameters of the K_v values determined in the laboratory for the 12 soil types constituting the aquifer (VAR = variance; SD = standard deviation; SE = standard error; VC = variation coefficient)

Parameter	Value
N	12
Min (m/s)	2.66e-6
Max (m/s)	3.44e-3
Mean (m/s)	3.97e-4
VAR (m²/s²)	9.36e-7
SD (m/s)	9.68e-4
SE (m/s)	2.79e-4
VC	2.44
Kurtosis	11.41
Skewness	3.35

Table 4 reports the piezometers associated with each sector corresponding to the directions from D1 to D8 (see Fig. 7), as previously described.

Hydraulic conductivity was measured both in the laboratory on samples of the individual mixtures defining the 12 considered soil types and directly on the unconfined heterogeneous aquifer through pumping tests. These tests were performed by pumping from the central well at the specified flow rates. The K values determined by the pumping tests are presented in the Supplementary Materials, specifically in Table SM1. It was not possible to determine these values for the A4 piezometer, which was only used to verify the maintenance of the hydraulic head in undisturbed initial conditions, and for the A7 piezometer, where the pressure transducer malfunctioned. Moreover, it was not possible to obtain the K values for piezometers placed at a distance where no change in the hydraulic head was detected. This particular situation occurred exclusively for the lowest considered pumping rate of 20 L/h and affected piezometers A3, A10, B3, B6, B9, B12, and B15, where no change in the hydraulic head was observed at this specific pumping rate. The values of the main statistical parameters of K at each well or piezometer location are displayed in Table SM2 of the Supplementary Materials [64]. For each piezometer, these statistical parameters were calculated based on 10 hydraulic conductivity values corresponding to the considered flow rates.

The K values reported in Table SM1 were determined through pumping tests, and thus represent horizontal hydraulic conductivity (K_h) values. Moreover, vertical

Table 5 Vertical hydraulic conductivity (K'_v) values determined at each well or piezometer

Wells/piezometers	K'_v (m/s)	Wells/piezometers	K'_v (m/s)
PW	6.59e-4	B4	1.31e-4
A1	7.3e-4	B5	1.02e-4
A2	1.51e-4	B6	1.74e-4
A3	6.03e-4	B7	6.15e-4
A5	1.22e-3	B8	7.21e-4
A6	1.1e-5	B9	1.24e-3
A8	1.29e-4	B10	7.23e-4
A9	125e-4	B11	7.16e-4
A10	1.04e-4	B12	6.22e-4
A11	6.5e-4	B13	1.41e-4
A12	1.27e-4	B14	1.27e-3
A13	6.09e-4	B15	1.39e-4
A14	4.12e-4	B16	5.18e-5
A15	6.12e-4	B17	9.18e-5
A16	1.51e-4	B18	1.49e-4
B1	6.4e-4	B19	3.57e-4
B2	6.07e-4	B20	6.2e-4
B3	1.16e-4	B21	1.22e-4

Table 6 Main statistical parameters of the K'_v values (VAR = variance; SD = standard deviation; SE = standard error; VC = variation coefficient)

Parameter	Value
N	36
Min (m/s)	1.10e-5
Max (m/s)	1.27e-3
Mean (m/s)	4.35e-4
VAR (m^2/s^2)	1.26e-7
SD (m/s)	3.54e-4
SE (m/s)	5.91e-5
VC	0.82
Kurtosis	0.00791
Skewness	0.81775

hydraulic conductivity (K'_v) was determined for each piezometer, calculated as the average of the K_v values associated with the individual cells intersected by the piezometer axis (see, Fig. 6). These values are presented in Table 5.

The main statistical parameters for the K'_v values were also calculated and are presented in Table 6 [64].

To investigate if the heterogeneity of the considered porous medium led to anisotropy in hydraulic conductivity, the anisotropy ratio ρ_a values were calculated using the known K_h and K'_v values. The parameter ρ_a was determined using Eq. (7), and the corresponding values for each well or piezometer are reported in Table SM3 of the Supplementary Materials. An in-depth statistical analysis was performed on ρ_a by calculating the main statistical

parameters corresponding to each considered pumping rate [64]. The values for these parameters can be found in Table SM4.

4.1 Verification of the hydraulic conductivity *(K)* scaling behavior

The scaling behavior of the hydraulic conductivity *(K)* was investigated for the aquifer under study in directions from D1 to D8, referencing Fig. 7. For each of these directions, pertaining to the sectors defined earlier, and for each considered pumping rate, the scaling laws $K = K(r)$ were established based on relation (9). The values of the respective parameters *a* and *b*, along with the corresponding determination coefficients (R^2), can be found in the Supplementary Materials, specifically in Table SM5. The R^2 coefficient provides a measure of how well observed outcomes are replicated by the model.

Always in Table SM5, cases where the scaling behavior of *K* was not sufficiently evident, for all the pumping rates and directions considered, are highlighted by displaying the value of (R^2) in italics. Similarly, instances where the scaling behavior of *K* was found to be practically non-existent are emphasized by presenting the values of (R^2) in both italics and bold. The following Fig. 8, as an example, depicts the scaling laws for the eight investigated directions, corresponding to a pumping rate of 35 L/h. The analogous representations of the scaling laws determined for the other pumping rates can be found in the Supplementary Material (Figure SM5).

5 Discussion

The high heterogeneity of the aquifer examined in this study, resulting from its construction process, is reflected in the values of the main parameter characterizing water flow, specifically the hydraulic conductivity *K*, as shown in Table SM1 of the Supplementary Materials. From Fig. 9 it can be observed that the logarithmic variance (VAR) for most of the K_h value series (see, Table SM2), obtained from individual piezometers through pumping tests with various rates, is lower than that associated with the series of K_v values determined in the laboratory using sample measurements (see, Table 3).

This pattern is also observed for the standard deviation (SD), standard error (SE), and variation coefficient (VC). Regarding the Kurtosis index, it is worth noting that in some cases for the series of hydraulic conductivity values K_h related to pumping tests, the index presents negative values. This suggests that the probability density function (pdf) curves for these series are flatter than the normal distribution. Conversely, in most cases, as is also true

Fig. 8 Scaling laws $K = K(r)$ for the directions (sectors) from D1 to D8, corresponding to K values associated with a pumping rate of 35 L/h
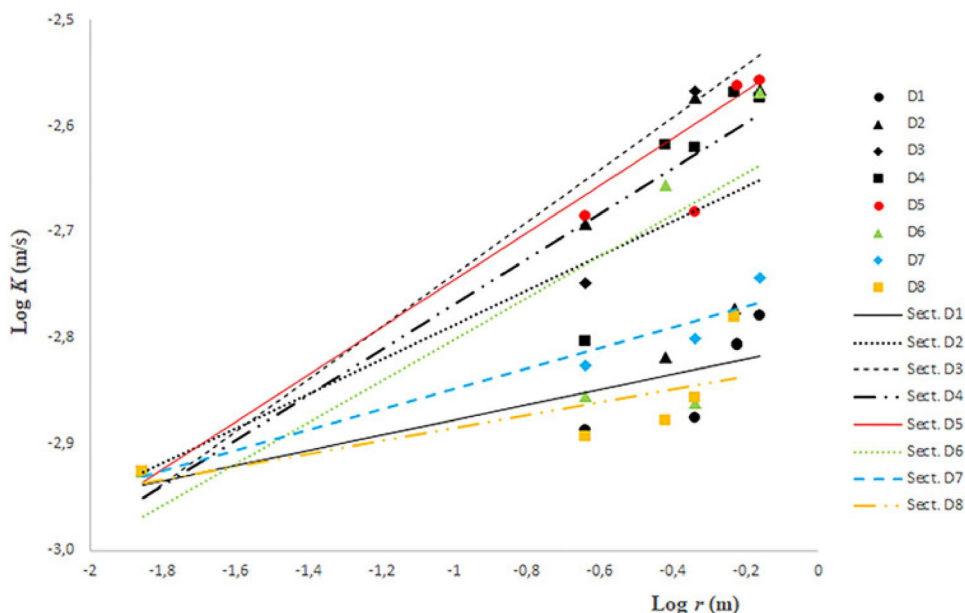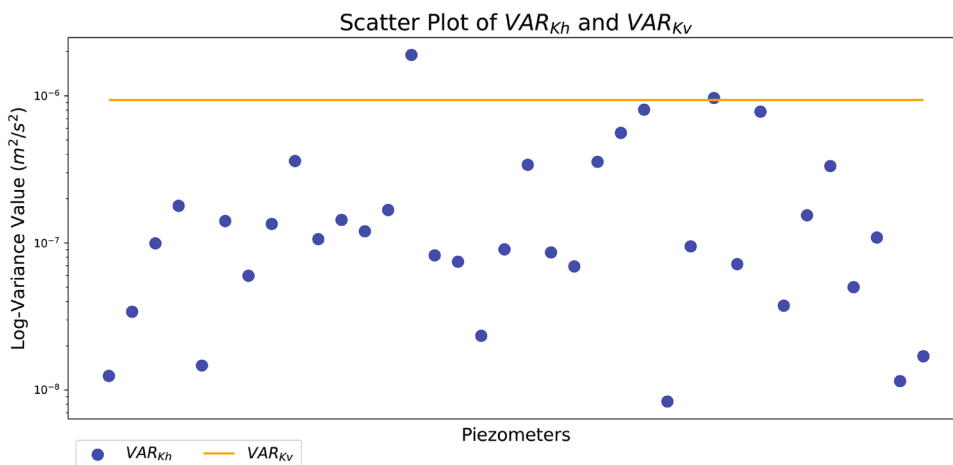

Fig. 9 Comparison in logarithmic scale between the variance VAR_{Kv} determined from soil samples and VAR_{Kh} determined for each piezometer

for the K_v values obtained from laboratory samples, the Kurtosis values are positive, and the pdf curves are less flat compared to the normal distribution. The Skewness index is positive for nearly all the tests performed in the piezometers, as indicated in Table SM2, and also for the value reported in Table 3 concerning the samples measurements, denoting a right-side asymmetry of the pdf curve with respect to the mean value. The average hydraulic conductivity values presented in Table SM2 exceed the average value associated with laboratory measurements on soil samples (see Table 3). Moreover, comparing the K_v' values in Table 5 with the K_h values in Table SM1 reveals that the K_v' values are significantly lower than the horizontal K_h values. This finding is also emphasized in Fig. 10, where the K_v' values for each

piezometer are compared with the K_h values obtained by averaging for each considered pumping rate.

Furthermore, while examining the statistical data in Table 6 and those in Table SM2, it can be observed that the variance, standard deviation, and standard error values of K_v' are of the same order of magnitude as those of K_h. The coefficient of variation for the K_v' values, although it is of the same order of magnitude, assumes lower values than the same coefficient for the K_h values. This vertical anisotropy, characterizing the entire aquifer due to various factors including the strong heterogeneity of the porous medium, is also emphasized by the ρ_a values in Table SM3 of the Supplementary Materials. The high mean values of ρ_a, along with the values of variance, standard deviation, standard error, and coefficient of variation shown in Table SM4, provide clear evidence of the pronounced anisotropy
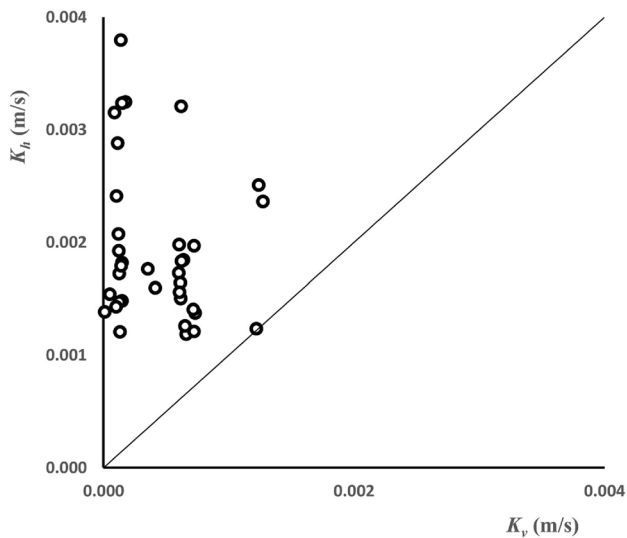
Fig. 10 Comparison of K'_v and K_h for each piezometer

Fig. 11 Distribution of K values in the studied aquifer for a pumping rate of 35 L/h

of the porous medium constituting the studied aquifer. Regarding its directional anisotropy, the scaling behavior of hydraulic conductivity was investigated, considering it as a representative parameter of water flow within the aquifer. The extreme variability of the scaling laws determined in the different directions emerges clearly in the example reported in Fig. 8 and in Figure SM5 of the Supplementary Materials. This circumstance is supported by the parameter values in Table SM5 which reveal the varying modes of K as r changes, in different directions, from D1 to D8. Additionally, referring to the R^2 coefficient values for individual scaling laws and each pumping rate as reported in Table SM5, it can be observed that the various scaling laws offer differing and more or less reliable representations across the considered directions. This finding indicates an evident scaling behavior of hydraulic conductivity for the investigated aquifer, resulting from its high heterogeneity. Specifically, it can be stated that the most reliable scaling laws are those related to direction D3, followed by those related to direction D5, and then those related to D4, and so on, in descending order, in directions D2, D1, D7, D8, and D6. In support of this observation, it can be seen from Table SM2 that the variance, standard deviation, standard error, and coefficient of variation values are the largest precisely in directions D6, D7, and D8. For the pumping rate of 35 L/h, the graph in Fig. 8 appears to demonstrate that the directions with higher hydraulic conductivity values correspond to scaling laws represented by straight lines with the steepest slopes, and vice versa. As an example, Fig. 11 illustrates the distribution of K values, measured across the entire examined aquifer via pumping tests with a flow rate of 35 L/h.
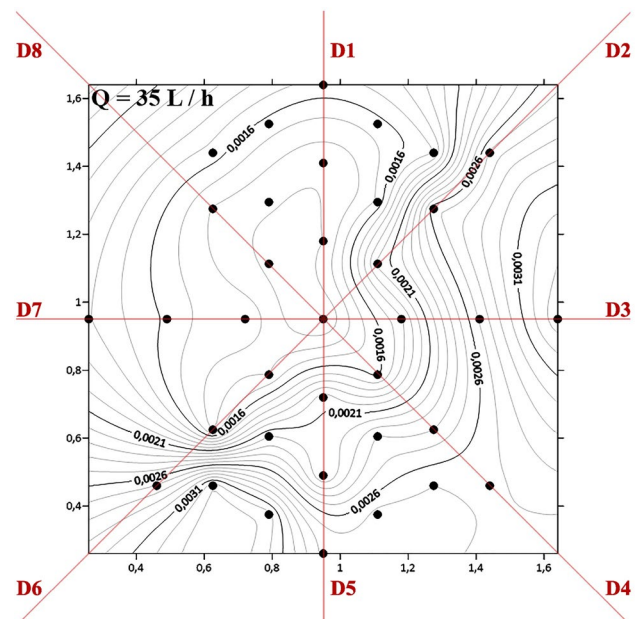
The main parameters of the geostatistical analysis related to the distribution of K depicted in Fig. 11 ($Q = 35 L/h$) are summarized in Table 7 [65, 66].

The K distribution displayed in Fig. 11 was obtained using ordinary kriging, considering a Spherical variogram model with a tendency toward stationarity for a value equal to 1.2 m and a sill value equal to $4.73 \cdot 10^{-7}$. All the K distributions related to the considered pumping rates for the tests, along with their respective variograms and geostatistical analysis parameters, can be found in the Supplementary Materials (Figure SM6; SM7; Table SM6) [65, 66]. Keeping as a reference example the flow rate of 35 L/h, Fig. 11 reveals that the highest values of K, and consequently the most significant variations of this parameter, occur along direction D3. Additionally, Fig. 8 shows high values of K in directions D5, D4, D2, and D6. Lower values of K are detected in directions D7, D8, and D1. Therefore, it can be

Table 7 Main parameters of the geostatistical analysis related to the distributions of K for a pumping rate of 35 L/h

Q	L/h	35
	(m^3/s)	9.72e-6
Variogram type		Spherical
Lag size		0.043369
Number of lags		32
Sill		6.15e-7
Range (m)		1.2
Cross validation: Root mean square		3.39e-4

concluded that the directions (or sectors) where the most significant variations of K with r occur are D2, D3, D5, and D6. Specifically, it is worth noting that direction D6 exhibits scaling laws $K = K(r)$ with less reliability, i.e., with lower R^2 values (see Table SM5). Furthermore, this direction D6 is also among those presenting less acceptable values of variance and variation coefficient of K measured in the piezometers (see Table SM2). It is worth noting that the heterogeneity's anisotropy of the aquifer produces a change of the radius of influence (R). As a consequence, the hydraulic gradients change, therefore determining a radial asymmetry in the cone of depression.

As an example, for the same flow rate of 35 L/h referenced in Fig. 11, the values of the radius of influence (R) in directions D1, D3, D5, and D7 were determined as previously specified in Sect. 3.3. These R values, shown in Table 8, exhibit substantial agreement with the distribution of the K values depicted in Fig. 11.

Another crucial aspect of this study is the importance of defining the heterogeneity scale and its influence on the evaluation of parameters describing water flow in porous media. Indeed, considering the measurements of K_v conducted on samples representing the soil types constituting the studied aquifer (Table 2), these values are undoubtedly measured at the laboratory scale. Examining Table 2, it is evident that the K_v values vary greatly, with an order of magnitude ranging from 10^{-6} m/s to 10^{-3} m/s.

Even considering the K_v' values reported in Table 5, which are determined as averages of the representative K_v values of individual cells intercepted by the vertical axis of each piezometer, these values still exhibit a substantial variation in orders of magnitude, ranging from 10^{-3} to 10^{-5}, despite the averaging effect. Although they are averaged, the K_v' values in Table 5 are based on measurements performed at the laboratory scale.

In contrast, when examining the K_h values in Table SM1 of the Supplementary Materials, determined in each piezometer as an average of three pumping tests for each flow rate considered, it is observed that all values in this table, although different from one another, share the same order of magnitude equal to 10^{-3}. These values were determined on the aquifer reproduced in the experimental device under examination, representing an intermediate scale between the laboratory and the field ones, and thus larger than the laboratory scale. The greater order of

magnitude of K at the investigation scale (10^{-3}) compared to those found at that of laboratory can be attributed to the fact that the values in Table SM1 represent horizontal hydraulic conductivity, while those in Tables 2 and 5 represent vertical hydraulic conductivity. However, the reduced variability of the hydraulic conductivity values in Table SM1, as evidenced by the consistent order of magnitude, suggests a tendency to converge towards a single value, which is likely to be reached at an even larger scale, i.e., that of field. This observation strongly aligns with numerous studies on the influence of heterogeneity at different scales on the homogeneity and anisotropy of a porous medium. These studies propose that a medium can appear homogeneous and isotropic at a scale larger than its heterogeneity scale, which often contributes to anisotropy as well [11, 13, 67]. Undoubtedly, in our investigation, the heterogeneity scale is that of laboratory, while the mesoscale of the aquifer on which the experimental investigation was conducted is larger, so the obtained results confirm the above assertion. By transitioning from the laboratory scale to the investigated mesoscale, the aquifer exhibited a tendency towards homogeneity, which is presumably expected to be achieved at an even larger scale, such as that of field.

6 Conclusions

Real aquifers exhibit significant heterogeneity, emphasizing the critical need to investigate the effects of such feature on flow and transport processes within porous media. The current research focused on a highly heterogeneous porous medium, specifically constructed in the laboratory. This aquifer comprised seven layers of porous materials, with each layer containing 361 cells of 12 randomly chosen soil types. The construction methods employed in this study render the findings particularly relevant, especially considering the scarcity of experimental models designed to examine such high degrees of heterogeneity.

One key finding of this study is the observation that strong heterogeneity led to pronounced anisotropy in the aquifer. The scale of investigation played a crucial role, as it provided detailed knowledge of the porous medium's properties, which is typically unattainable for larger aquifers. For instance, this detailed knowledge enabled the determination of vertical hydraulic conductivity and anisotropy at the central well and various piezometers. Anisotropy ratios were calculated, and it was found that the K_v' values at each piezometer were consistently lower than the K_h values determined at the same locations by pumping tests. This observation underscored the vertical anisotropy of the aquifer, resulting from its construction methods and high heterogeneity.

Table 8 Values of the radius of influence (R) for directions D1, D3, D5, D7, and for a pumping rate of 35 L/h

Directions	R (m)
D1	0.78488
D3	0.91489
D5	0.89286
D7	0.82350

Directional anisotropy was also verified by determining the scaling laws $K = K(r)$ in the directions (sectors) from D1 to D8, as depicted in Fig. 7, and can be attributed to the same factors. These scaling laws, as shown in Table SM5, exhibit varying degrees of representativeness in individual directions, emphasized by the corresponding R^2 values. The study demonstrated that a highly heterogeneous porous medium at the laboratory scale tends to exhibit homogeneity and, consequently, isotropy at a larger scale, such as the scale of the considered aquifer. The comparison between hydraulic conductivity values in Table 2 (laboratory scale) and Table SM1 (investigation mesoscale) highlights this trend towards homogeneity and isotropy at larger scales. This observation aligns with the findings of various authors [11, 13, 67], further emphasizing the importance of considering heterogeneity and scale when investigating flow and transport phenomena in porous media.

The distinctive results of this experimental study stem from the specially-built laboratory device that simulates a highly heterogeneous phreatic aquifer. In addition to the main findings, this research accomplished other objectives, such as verifying the scaling behavior of K and providing new data for the scientific community.

More studies in this direction are desirable to ensure that theoretical and conceptual outcomes are supported by robust experimental confirmation. There are numerous aspects to explore regarding highly heterogeneous aquifers, all of which are of significant interest. Among these, in future projects, it will be fundamental to investigate the role of heterogeneity and anisotropy under unsaturated water flow conditions.

Declarations

Conflict of interest The authors declare no conflict of interest.

References

1. Bear J (2013) Dynamics of fluids in porous media. Dover Publications, New York
2. Dagan G (1989) Flow and transport in porous formations, 1st edn. Springer, Berlin
3. Severino G, Cvetkovic V, Coppola A (2005) On the velocity covariance for steady flows in heterogeneous porous formations and its application to contaminants transport. Comput Geosci 9(4):155–177. https://doi.org/10.1007/S10596-005-9005-3
4. Severino G, Santini A (2005) On the effective hydraulic conductivity in mean vertical unsaturated steady flows. Adv Water Resour 28(9):964–974. https://doi.org/10.1016/J.ADVWATRES.2005.03.003
5. Severino G, Comegna A, Coppola A, Sommella A, Santini A (2010) Stochastic analysis of a field-scale unsaturated transport experiment. Adv Water Resour 33(10):1188–1198. https://doi.org/10.1016/J.ADVWATRES.2010.09.004
6. Severino G (2011) Stochastic analysis of well-type flows in randomly heterogeneous porous formations. Water Resour Res 47(3):3520. https://doi.org/10.1029/2010WR009840
7. Severino G, Leveque S, Toraldo G (2019) Uncertainty quantification of unsteady source flows in heterogeneous porous media. J Fluid Mech 870:5–26. https://doi.org/10.1017/JFM.2019.203
8. Fallico C, De Bartolo S, Veltri M, Severino G (2016) On the dependence of the saturated hydraulic conductivity upon the effective porosity through a power law model at different scales. Hydrol Process 30(13):2366–2372. https://doi.org/10.1002/HYP.10798
9. Fallico C, De Bartolo S, Troisi S, Veltri M (2010) Scaling analysis of hydraulic conductivity and porosity on a sandy medium of an unconfined aquifer reproduced in the laboratory. Geoderma 160(1):3–12. https://doi.org/10.1016/J.GEODERMA.2010.09.014
10. Severino G, Santini A, Monetti VM (2009) Modelling water flow and solute transport in heterogeneous unsaturated porous. Media 25:361–383. https://doi.org/10.1007/978-0-387-75181-8_17
11. Clavaud JB, Maineult A, Zamora M, Rasolofosaon P, Schlitter C (2008) Permeability anisotropy and its relations with porous medium structure. J Geophys Res Solid Earth 113(B1):1202. https://doi.org/10.1029/2007JB005004
12. Dagan G, Lessoff SC (2007) Transmissivity upscaling in numerical aquifer models of steady well flow: unconditional statistics. Water Resour Res. https://doi.org/10.1029/2006WR005235
13. Dagan G (1986) Statistical theory of groundwater flow and transport: pore to laboratory, laboratory to formation, and formation to regional scale. Water Resour Res 22(9S):120S-134S. https://doi.org/10.1029/WR022I09SP0120S

14. Ojala IO, Ngwenya BT, Main IG (2004) Loading rate dependence of permeability evolution in porous aeolian sandstones. J Geophys Res Solid Earth. https://doi.org/10.1029/2002JB002347

15. Vajdova V, Baud P, Wong T-F (2004) Permeability evolution during localized deformation in Bentheim sandstone. J Geophys Res Solid Earth 109(B10):10406. https://doi.org/10.1029/2003JB002942

16. Wright HMN, Roberts JJ, Cashman KV (2006) Permeability of anisotropic tube pumice: model calculations and measurements. Geophys Res Lett. https://doi.org/10.1029/2006GL027224

17. Bouma J (1982) Measuring the hydraulic conductivity of soil horizons with continuous macropores. Soil Sci Soc Am J 46(2):438–441. https://doi.org/10.2136/SSSAJ1982.03615995004600020047X

18. Chandler MA, Kocurek G, Goggin DJ, Lake LW (1989) Effects of stratigraphic heterogeneity on permeability in Eolian sandstone sequence, Page Sandstone, Northern Arizona. AAPG Bull 73(5):658–668. https://doi.org/10.1306/44B4A249-170A-11D7-8645000102C1865D

19. Fallico C, De Bartolo S, Brunetti GFA, Severino G (2020) Use of fractal models to define the scaling behavior of the aquifers' parameters at the mesoscale. Stoch Environ Res Risk Assess. 35(5):971–984. https://doi.org/10.1007/S00477-020-01881-2

20. Ghanbarian B, Hunt AG, Ewing RP, Sahimi M (2012) Tortuosity in porous media: a critical review. Soil Sci Soc Am J 77(5):1461–1477. https://doi.org/10.2136/SSSAJ2012.0435

21. Giménez D, Rawls WJ, Lauren JG (1999) Scaling properties of saturated hydraulic conductivity in soil. Geoderma 88(3–4):205–220. https://doi.org/10.1016/S0016-7061(98)00105-0

22. Indelman P, Dagan G (2006) Modelling of regional-scale wellflow in heterogeneous aquifers: 2-D or not 2-D? In: Proceedings of ModelCARE'2005, Vol. 304, international association of hydrological sciences, IAHS, The Hague, The Netherlands, pp 215–219

23. Knudby C, Carrera J (2006) On the use of apparent hydraulic diffusivity as an indicator of connectivity. J Hydrol 329(3–4):377–389. https://doi.org/10.1016/J.JHYDROL.2006.02.026

24. Yanuka M, Dullien FA, Elrick DE (1986) Percolation processes and porous media: I. Geometrical and topological model of porous media using a three-dimensional joint pore size distribution. J Colloid Interface Sci 112(1):24–41. https://doi.org/10.1016/0021-9797(86)90066-4

25. Dagan G, Lessoff SC, Fiori A (2009) Is transmissivity a meaningful property of natural formations? Conceptual issues and model development. Water Resour Res 45(3):3425. https://doi.org/10.1029/2008WR007410

26. Severino G, Monetti VM, Santini A, Toraldo G (2006) Unsaturated transport with linear kinetic sorption under unsteady vertical flow. Transp Porous Media 63(1):147–174. https://doi.org/10.1007/S11242-005-4424-0

27. Indelman P (2004) On macrodispersion in uniform—radial divergent flow through weakly heterogeneous aquifers. Stoch Environ Res Risk Assess 18(1):16–21. https://doi.org/10.1007/S00477-003-0165-1

28. Severino G, Fallico C, Brunetti GFA (2024) Correlation structure of steady well-type flows through heterogeneous porous media: results and application. Water Resour Res 60(2):e2023WR036279. https://doi.org/10.1029/2023WR036279

29. Sánchez-Vila X, Axness CL, Carrera J (1999) Upscaling transmissivity under radially convergent flow in heterogeneous media. Water Resour Res 35(3):613–621. https://doi.org/10.1029/1998WR900056

30. Sanchez-Vila X, Tartakovsky DM (2007) Ergodicity of pumping tests. Water Resour Res 43:3414. https://doi.org/10.1029/2006WR005241

31. Severino G, De Bartolo S, Brunetti GFA, Sommella A, Fallico C (2019) Experimental evidence of the stochastic behavior of the conductivity in radial flow configurations. Stoch Environ Res Risk Assess 33(8):1651–1657. https://doi.org/10.1007/S00477-019-01704-Z

32. Brunetti GFA, Fallico C, De Bartolo S, Severino G (2022) Well-type steady flow in strongly heterogeneous porous media: an experimental study. Water Resour Res 5:e2021WR030717. https://doi.org/10.1029/2021WR030717

33. Indelman P, Fiori A, Dagan G (1996) Steady flow toward wells in heterogeneous formations: mean head and equivalent conductivity. Water Resour Res 32(7):1975–1983. https://doi.org/10.1029/96WR00990

34. Neuman SP, Tartakovsky DM, Wallstrom TC, Winter CL (1996) Correction to "Prediction of steady state flow in nonuniform geologic media by conditional moments: exact nonlocal formalism, effective conductivities, and weak approximation" by Shlomo P. Neuman and Shlomo Orr. Water Resour Res 32(5):1479–1480. https://doi.org/10.1029/96WR00489

35. Severino G (2011) Macrodispersion by point-like source flows in randomly heterogeneous porous media. Transp Porous Media 89(1):121–134. https://doi.org/10.1007/S11242-011-9758-1

36. Rubin Y (2003) Applied stochastic hydrogeology. Oxford University Press. https://doi.org/10.1093/OSO/9780195138047.001.0001

37. Indelman P (1996) Averaging of unsteady flows in heterogeneous media of stationary conductivity. J Fluid Mech 310:39–60. https://doi.org/10.1017/S0022112096001723

38. Severino G, Santini A, Sommella A (2008) Steady flows driven by sources of random strength in heterogeneous aquifers with application to partially penetrating wells. Stoch Environ Res Risk Assess 22(4):567–582. https://doi.org/10.1007/S00477-007-0175-5

39. Renard P, De Marsily G (1997) Calculating equivalent permeability: a review. Adv Water Resour 20(5–6):253–278. https://doi.org/10.1016/S0309-1708(96)00050-4

40. Schneider CL, Attinger S (2008) Beyond Thiem: a new method for interpreting large scale pumping tests in heterogeneous aquifers. Water Resour Res 44(4):4427. https://doi.org/10.1029/2007WR005898

41. Severino G, Coppola A (2012) A note on the apparent conductivity of stratified porous media in unsaturated steady flow above a water table. Transp Porous Media 91(2):733–740. https://doi.org/10.1007/S11242-011-9870-2

42. Fallico C, Ianchello M, De Bartolo S, Severino G (2018) Spatial dependence of the hydraulic conductivity in a well-type configuration at the mesoscale. Hydrol Process 32(4):590–595. https://doi.org/10.1002/HYP.11422

43. Brunetti GFA, Lauria A, Fallico C (2021) Comparison among variation models of the hydraulic conductivity with the effective porosity in confined aquifer. IOP Conf Ser Earth Environ Sci 1:012003. https://doi.org/10.1088/1755-1315/958/1/012003

44. Brunetti GFA, De Bartolo S, Fallico C, Frega F, Rivera Velásquez MF, Severino G (2021) Experimental investigation to characterize simple versus multi scaling analysis of hydraulic conductivity at a mesoscale. Stoch Environ Res Risk Assess. https://doi.org/10.1007/S00477-021-02079-W/FIGURES/9

45. Comegna A, Coppola A, Comegna V, Severino G, Sommella A, Vitale CD (2010) State-space approach to evaluate spatial variability of field measured soil water status along a line transect in a volcanic-vesuvian soil. Hydrol Earth Syst Sci 14(12):2455–2463. https://doi.org/10.5194/HESS-14-2455-2010

46. Severino G, Santini A, Sommella A (2003) Determining the soil hydraulic conductivity by means of a field scale internal

drainage. J Hydrol 273(1–4):234–248. https://doi.org/10.1016/S0022-1694(02)00390-6

47. Fernàndez-Garcia D, Illangasekare TH, Rajaram H (2004) Conservative and sorptive forced-gradient and uniform flow tracer tests in a three-dimensional laboratory test aquifer. Water Resour Res 40(10):10103. https://doi.org/10.1029/2004WR003112

48. Lambe T (1951) Soil testing for engineers. Wiley, New York

49. Danielson RE, Sutherland PL (1986) Porosity. In: Klute A (ed), Methods of soil analysis, part 1. physical and mineralogical methods—agronomy monograph, 2nd edn., vol. 9. American Society of Agronomy-Soil Science Society of America, Madison, WI, USA, Ch. 18, pp 443–461. https://doi.org/10.2136/SSSABOOKSER5.1.2ED.C18

50. Staub M, Galietti B, Oxarango L, Khire MV, Gourc J-P (2009) Porosity and hydraulic conductivity of MSW using laboratoryscale tests. In: Proceedings of the 3rd international workshop "hydro-physico-mechanics of landfills", Braunschweig

51. Ahuja LR, Cassel DK, Bruce RR, Barnes BB (1989) Evaluation of spatial distribution of hydraulic conductivity using effective porosity data. Soil Sci 148(6):404–411

52. Klute A, Dirksen C (1986) Hydraulic conductivity and diffusivity: laboratory methods. In: Klute A (ed.), Methods of soil analysis, Part 1: physical and mineralogical methods - agronomy monograph, 2nd edn., vol 9, American Society of Agronomy-Soil Science Society of America, Madison, WI, USA, Ch. 28, pp 687–734. https://doi.org/10.2136/SSSABOOKSER5.1.2ED.C28

53. Pliakas F, Petalas C (2011) Determination of hydraulic conductivity of unconsolidated river alluvium from permeameter tests, empirical formulas and statistical parameters effect analysis. Water Resour Manag 25(11):2877–2899. https://doi.org/10.1007/S11269-011-9844-8

54. Vienken T, Dietrich P (2011) Field evaluation of methods for determining hydraulic conductivity from grain size data. J Hydrol 400(1–2):58–71. https://doi.org/10.1016/J.JHYDROL.2011.01.022

55. Neuman SP (1972) Theory of flow in unconfined aquifers considering delayed response of the water table. Water Resour Res 8(4):1031–1045. https://doi.org/10.1029/WR008I004P01031

56. Cooper HH, Jacob CE (1946) A generalized graphical method for evaluating formation constants and summarizing well-field history. Trans-Am Geophys Union 27(534):526

57. Neuman SP, Orr S (1993) Prediction of steady state flow in nonuniform geologic media by conditional moments: Exact nonlocal formalism, effective conductivities, and weak approximation. Water Resour Res 29(2):341–364. https://doi.org/10.1029/92WR02062

58. Sánchez-Vila X (1997) Radially convergent flow in heterogeneous porous media. Water Resour Res 33(7):1633–1641. https://doi.org/10.1029/97WR01001

59. Jacob CE (1940) On the flow of water in an elastic artesian aquifer. Ann Geophys Union Trans pt 2:574–586

60. Duffield GM (2007) AQTESOLV for Windows Version 4.5 User's Guide

61. Bear J (1979) Hydraulics of groundwater. McGraw-Hill International Book Company, New York

62. Schulze-Makuch D, Cherkauer DS (1998) Variations in hydraulic conductivity with scale of measurement during aquifer tests in heterogeneous, porous carbonate rocks. Hydrogeol J 6(2):204–215. https://doi.org/10.1007/S100400050145

63. Schulze-Makuch D, Carlson DA, Cherkauer DS, Malik P (1999) Scale dependency of hydraulic conductivity in heterogeneous media. Groundwater 37(6):904–919. https://doi.org/10.1111/J.1745-6584.1999.TB01190.X

64. Mosteller F, Tukey JW (1977) Data analysis and regression. Addison-Wesley, Boston

65. Matheron G (1963) Principles of geostatistics. Econ Geol 58(8):1246–1266. https://doi.org/10.2113/GSECONGEO.58.8.1246

66. Chiles JP, Delfiner P (1999) Geostatistics : modeling spatial uncertainty, 1st edn. Wiley-Interscience, New York. https://doi.org/10.1007/978-3-642-75015-1

67. Bernabé Y (1992) On the measurement of permeability in anisotropic rocks. In: Brian E, Teng-fong W (eds), Fault mechanics and transport properties of rocks, 1st Edn, vol 51. Academic Press, London, Ch. 6, pp 147–167. https://doi.org/10.1016/S0074-6142(08)62821-1